Available online at www.sciencedirect.com
ScienceDirect
Trans. Nonferrous Met. Soc. China 24(2014) 975−981
Transactions of Nonferrous Metals Society of China
www.tnmsc.cn

Evolution of microstructure and hardness of aluminum after friction stir processing

Wen-ying GAN, Zheng ZHOU, Hang ZHANG, Tao PENG

College of Materials Science and Engineering, Chongqing University, Chongqing 400044, China

Received 20 March 2013; accepted 11 September 2013

Abstract: The effects of friction stir processing (FSP) on the microstructure, microtexture and hardness of rolled pure aluminum were investigated. The microstructure and microtexture were characterized using electron backscattered diffraction (EBSD) technique on the transversal section. The stir zone (SZ) contains fine, equiaxed and fully recrystallized grains. The texture component of the base material mainly consists of R, S and brass R textures. Miner copper texture component is also determined. In the center of the stir zone, the dominant texture is (111) parallel to about 70° from ND pointing toward RD. The textures of this location rotating clockwise about 30° and anticlockwise about 60° around the ND result in the textures of the areas, which are 3 mm apart from this location on the retreating side and advancing side, respectively.

Key words: friction stir processing; aluminum; EBSD; texture

1 Introduction

As an important method for material strengthening through microstructure refinement, friction-stir processing (FSP) has shown significant microstructural modification and improved mechanical properties for aluminum and its alloys. During FSP, a rotating tool with a shoulder and a pin plunges into the surface of the plates which are processed and moves along the plates [1]. The shoulder contacts with the top surface of the workpiece tightly. The heat generated by the shoulder and the pin softens the material below its melting point around the pin. Severe plastic deformation and flow of this plasticization material occur as the tool is translated along the welding direction.

Four key zones have identified in a friction stir processed material [1−3]. They are: 1) unaffected material; 2) heat-affected zone (HAZ) which is only affected by the heat; 3) thermo-mechanically affected zone (TMAZ) lies between the HAZ and the stir zone (SZ), where material has undergone heat and plastic deformation; 4) stir zone which experiences the most severe deformation and temperature is recrystallized to form fine equiaxed grains. Although FSP has been widely used for material modification, the microstructural evolution to produce the final modified microstructure is still not well understood [4].

SATO et al [5] and SUHUDDIN [6] reported that the dominant texture was simple shear texture with the {111} parallel to the sheet surface after FSP of aluminum alloys. This type of texture was beneficial for enhanced formability. It was studied that the profile of hardness curve and “W” shape was obtained in aluminum alloys [7−11]. YADAV and BAURI [12] reported the effect of FSP on microstructural evolution and mechanical properties of cast aluminum. They proclaimed that the grain size was refined efficiently and the mechanical properties were improved after FSP. There are a number of previous studies characterizing the microstructure, and mechanical properties of various aluminum alloys produced by FSP, few reports are focused on pure aluminum, and studies about crystallographic texture of FSP pure aluminum are much more rare. It is also important to study the microstructure and mechanical properties of pure aluminum after FSP in order to understand the microstructure and mechanical properties developed without the effects of secondary phases. In this work, FSP was used to modify the microstructure of pure aluminum. The evolution of microstructure and microtexture after FSP was examined systematically in order to understand the deformation during FSP.

Corresponding author: Zheng ZHOU; Tel: +86-13206082181; E-mail: zhzheng6423@qq.com
DOI: 10.1016/S1003-6326(14)63151-4

Additionally, the hardness of the entire transversal section was also investigated to demonstrate the changes of mechanical properties.

2 Experimental

The base material used for this study was commercial pure (99.00%) aluminum plate containing iron and silicon (0.95%), copper (0.05%−0.20%), zinc (0.10%) and manganese (0.05%) as major impurities. The plate was cold rolled to a thickness of 2 mm. Single-pass FSP was carried out on the aluminum plate. A cylindrical probe was used with diameter of 5 mm and length of 1.65 mm. A cylindrical shoulder without thread was applied with diameter of 10 mm. The tool was operated with a back tilt of 2.5°, using a rotational speed of 800 r/min and a tool transverse speed of 200 mm/min along the rolling direction of the plate. The section of the plane perpendicular to the welding direction was cut and then polished and etched by Keller reagent to obtain an optical macrograph.

Detailed microstructure and microtexture analysis of the entire processed regions across the transversal section was undertaken using electron backscattered diffraction (EBSD). Specimens were cut from the friction stir processed tracks in the plate using electrical discharge machining (EDM). Then, they were mechanically ground and electropolished with a solution of 10% perchloric acid alcohol for 40 s at −20 °C with an applied potential of 20 V. EBSD studies were performed in a FEI Nova 400 FEG-SEM with step size of 0.5 and 0.3 μm for data collection, which were undertaken horizontally from the retreating side (RS) to the advancing side (AS). The regions were indicated by *a*−*h*, as shown in Fig. 1. EBSD maps were used to plot inverse pole figures, misorientation angle histograms and pole figures via the Channel 5 software from HKL technology. A hardness measurement extending across the entire region with a spacing of 0.5 mm was conducted using a Vickers indenter with 25 N load and 10 s dwelling time.

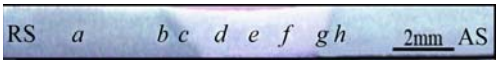

Fig. 1 Macrograph of transversal section perpendicular to RD direction of pure aluminum

3 Results and discussion

3.1 Microstructure

The typical macroscopic overview of the transversal section is indicated in Fig. 1. No defects are found on the processed regions. The basin-shaped stir zone is visible clearly and the SZ width exceeds the width of the probe. Many researchers [1,13] reported that the shape of the SZ is related with processing parameters, tool geometry, temperature of workpiece, and thermal conductivity of the material. The upper surface of the stir zone is wider than the bottom, because the upper surface experiences extreme deformation and frictional heating by contacting with a cylindrical-tool shoulder during FSP, yet the bottom is only affected by the pin. The entire processed zone is not symmetric between the AS and the RS. The slop of the boundary between the SZ and TMAZ is larger in the AS than those in the RS. It is attributed to the 2.5° back tilt of the tool, leading to the different plastic flow pattern between the AS and RS. It was observed that the boundary between SZ and TMAZ is more obvious in the AS than those in the RS, as reported in FSP of AA5182-O aluminum alloy [14].

Figure 2 shows the EBSD (IPF+GB) maps, obtained from the locations *a*−*h* respectively, as marked in Fig. 1. High-angle boundaries (>15°) are designated by black lines, and low-angle boundaries (from 2° to 15°) are designated by white lines. Location *e* is the center of the SZ. Locations *b*, *c* and *d* lie in the RS of the transversal section. Locations *b*, *c* and *d* are about 5.5, 4.5, and 3 mm away from the location *e*, respectively. Location *d* is in the SZ, and location *c* is just outside of the boundary between the SZ and TMAZ, while location *b* is in the HAZ. Locations *f*, *g* and *h* are in the AS of the transversal section. Locations *f*, *g* and *h* are about 5, 4 and 3 mm away from the location *e*, respectively. The specific location is the same as the RS.

The EBSD map of the base material is shown in Fig. 2(a), showing the typical rolled microstructures which are elongated grains with dense sub-structures in the grains. From Figs. 2(d)−(f), it can be observed that the microstructure of SZ is obviously different from that in the base material. The grains in the SZ are particularly small and equiaxed, which are attributed to the dynamic recrystallization during FSP as some researchers reported [15,16]. And the average grain size of locations *d*, *e* and *f* for grains defined by 5° misorientation, are approximately 2.97, 2.61 and 3.11 μm, respectively. The definite dynamic recrystallization mechanism has not been understood. Some researchers [17,18] proposed several typical recrystallization mechanisms including geometric dynamic recrystallization which can explain the phenomenon of this work preferably. The mechanism indicates that plastic deformation occurs in the grains in the form of shearing during FSP, making the BM with small and elongated grains divide into small equiaxed grains, as seen in the SZ. Figure 3 shows the misorientation angle histograms of locations *a*−*h*, and Table 1 shows the fraction of high angle boundaries. By comparing locations *d*, *e* and *f* to location *a*, it can be concluded that a much higher fraction of high angle

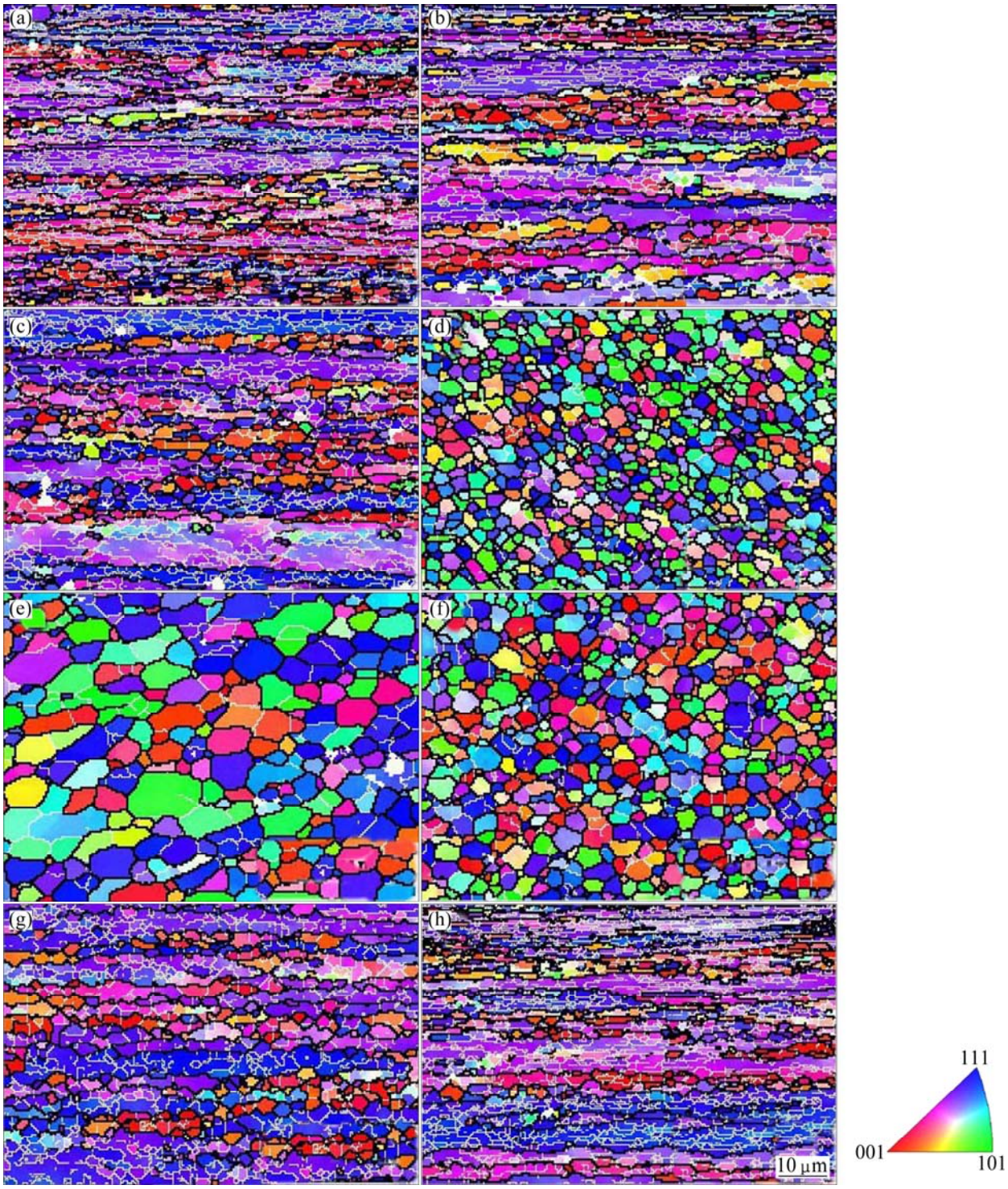

Fig. 2 EBSD maps (IPF+GB) with respect to ND for regions examined from different locations indicated in Fig. 1: (a) Location *a*; (b) Location *b*; (c) Location *c*; (d) Location *d*; (e) Location *e*; (f) Location *f*; (g) Location *g*; (h) Location *h*

boundaries (over 80%) exits in the SZ due to the dynamic recrystallization.

It can be discovered that the grain size of the location *d* is a little smaller than that of location *f*, which mainly results from the asymmetric material flow pattern between the centerline. Our research group has studied the material flow in 7075 aluminum alloy through "stop" action systematically, and indicated that some grains of the RS flow into the AS, along with the growth of the grains through absorbing sub-grains during the process. Therefore, it can be informed that the material flow of pure aluminum is roughly same as aluminum alloys during FSP, leading to the fact that the grain size of RS is smaller than that of AS. The fraction of high angel

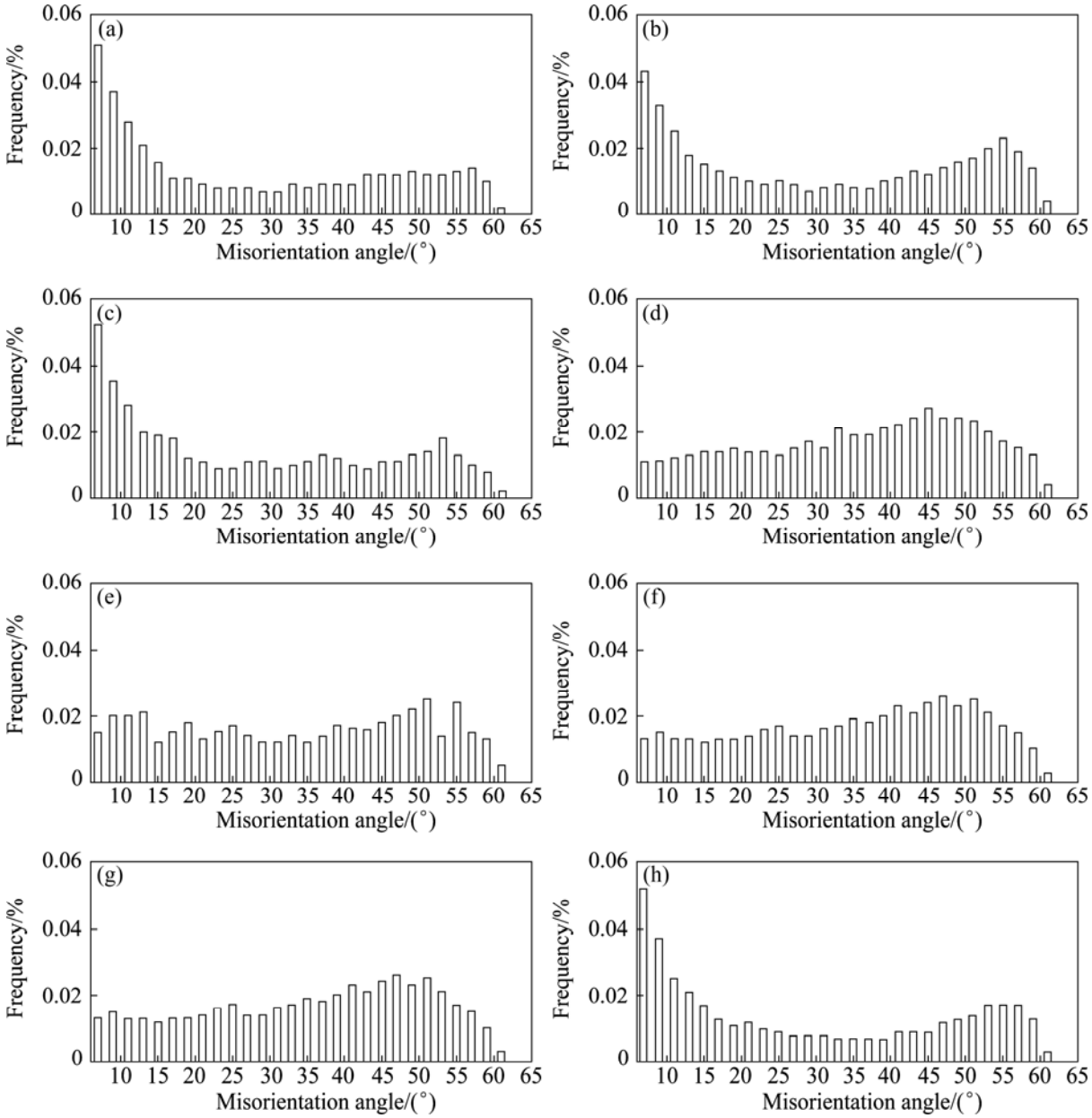

Fig. 3 Misorientation angle histograms for regions examined from different locations: (a) Location *a*; (b) Location *b*; (c) Location *c*; (d) Location *d*; (e) Location *e*; (f) Location *f*; (g) Location *g*; (h) Location *h*

boundary of the AS is slightly higher than that of the RS. During the grains are flowing into the AS from the RS, the sub-grains are absorbed by the growing grains, which leads to the growth of the grains. This phenomenon also can be confirmed by comparing Figs. 3(c)−(g) with Figs. 3(b)−(h), respectively. Locations *c* and *g* are the TMAZ regions which experience both temperature and deformation during FSP including elongated and equiaxed grains. Although the TMAZ undergoes plastic deformation, recrystallization does not occur entirely in this zone due to insufficient deformation strain. From Figs. 2(c) and (g), it can be found that there are many low angle boundaries in the grains. Figure 4 also shows that the fractions of high angle boundary of the TMAZ

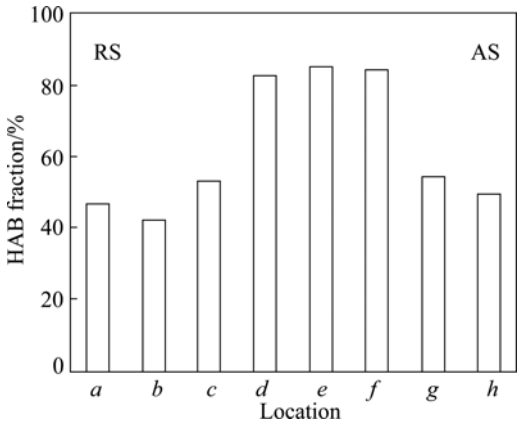

Fig. 4 Fractions of high-angle boundary for regions examined from *a* to *h*

are only 52.5% and 54.5% in the RS and AS, respectively. The two phenomena both indicate the partial recrystallization of the TMAZ. The average grain size of the two regions can not be measured accurately due to the disorder of the grains.

Beyond the TMAZ, in the HAZ, there is no plastic deformation, only a thermal cycle experiences in this zone. From Figs. 2(b) and (h), it can be discovered that the HAZ retains the same grain structure as the base material. It is also hard to know the size of the grains quantificationally because of its chaotic grain boundary distribution while the grain size is slightly larger than that of the base material due to the heat cycle.

The color code corresponds to the orientation of the grains. The EBSD (IPF+GB) map of base material, as shown in Fig. 2(a), shows ⟨111⟩//ND (blue), ⟨112⟩//ND (purple) and ⟨001⟩//ND (red) preferential orientations in the rolled base material, and the three preferential orientations present banded structure. Figures 2(d)−(f) indicate many small grains have no obvious preferential orientations emerging in the SZ. The ⟨111⟩//ND, ⟨112⟩//ND and ⟨001⟩//ND preferential orientations of the BM disappear in the SZ after FSP. Figures 2(c) and (g) show elongated grains intermixed with few equiaxed grains having the same preferential orientations as BM. Elongated grains are dominated by ⟨111⟩//ND and ⟨112⟩//ND orientations, but the equiaxed grains are dominated by ⟨001⟩//ND orientation due to the dynamic recrystallization. This phenomenon may indicate that recrystallization occurs in the ⟨001⟩//ND orientation preferentially and larger deformation happens in some regions, where sufficient energy could be supplied to initiate dynamic recrystallization. But some regions only experiencing heat cycle undergo less deformation due to the insufficient energy. This indicates the existence of strain gradient.

Detailed evolution of the materials during FSP could be revealed through microtexture patterns. Locations *a* to *h* throughout the transversal section, as shown in Fig. 1, are analyzed independently and the series of {111} pole figures are shown in Fig. 5 in order to recognize the formation of the deformation texture. There are two partial fiber textures after shear deformation in fcc metals [19]. One fiber is fiber A which can be denoted as {111}⟨*uvw*⟩, the other one is fiber B which can be denoted as {*hkl*}⟨110⟩. Besides, there has a metastable texture C which can be denoted as {110}⟨011⟩. Figure 5(a) shows the texture of the base material, revealing that the texture of the BM mainly consists of mixed R ({124}⟨211⟩), S and brass R ({236}⟨385⟩) texture. Miner copper texture is also discovered [20,21]. Compared with the BM, as shown in Figs. 5(b), (c), (g) and (h), the same type of texture is found in the TMAZ and HAZ, but the texture is less intense. Since the diameter of the tool is 10 mm, this illustrates that crystallite lattice orientations change little in the TMAZ and HAZ. Figure 5(e) shows the center of the SZ, demonstrating that the dominant orientation is (111) parallel to about 70° from ND pointing toward the direction of the RD. Similar orientations were discovered by FIELD et al [19], who proposed that the (111) was evolved from two primary orientations which were (111) pole aligned with ND whose ⟨110⟩ direction aligned with TD and (411) aligned with ND. From Figs. 5(d) and (f), the texture in locations *g* and *h* is much scattered. The texture of location *e* clockwise rotates about 30° and anticlockwise rotates about 60° around the ND, resulting in the texture of locations *d* and *f*, respectively. The SZ is

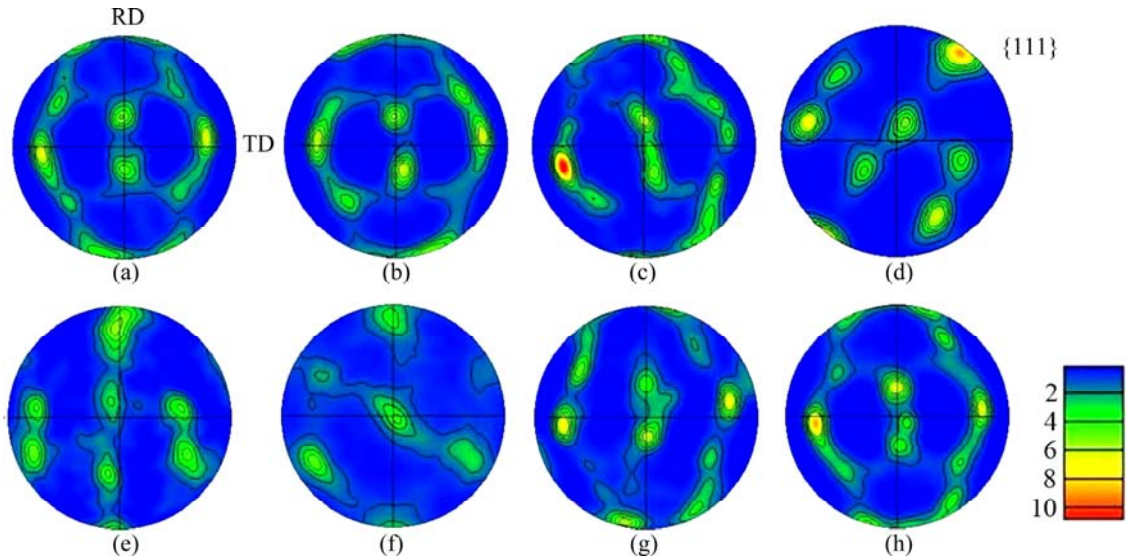

Fig. 5 (111) pole figures for different regions as shown in Fig. 1: (a) Location *a*; (b) Location *b*; (c) Location *c*; (d) Location *d*; (e) Location *e*; (f) Location *f*; (g) Location *g*; (h) Location *h*

mainly influenced by the rotated pin. During FSP, the pin rotates around the ND roughly, so the shear texture is formed around the ND in the SZ. Besides, the rotated pin induces shear stress, causing the production of shear stress at forward motion of the rotating pin as well. The two shear stresses are imposed on the SZ. The texture evolution in the SZ is affected by the composite shear stress. However, the shear stress is not symmetric between the AS and RS. At AS, the direction of the forward motion aligns with that of the tangent of the pin. But these directions are not fully the same, resulting in the complex shear stress and material flow. At RS, the direction of the forward motion is opposite to the direction of the tangent of the pin, which leads to more complex shear stress and material flow. So, complicated texture is produced by the complex shear stress and material flow at both AS and RS. Though the stress state is complicated, all shear stresses are perpendicular to the ND. The complex shear stress produces the complicated material flow and the {111} texture is finally obtained in the SZ after FSP. The {111} planes are approximately aligned with the sheet surface. And the {111} texture is beneficial to enhancing the formability of aluminum [21]. Therefore, we should try to achieve this type of texture through controlling the processing conditions.

3.3 Hardness

The hardness curve of the transversal section is shown in Fig. 6. The hardness of the base metal is found to be about HV31 and shows a horizontal line. The hardness curve shows a “U” shape. It can be observed that a local material softening occurs in the FSP zone because of the heat produced by the process of FSP. SATO et al [22] demonstrated that hardness is not actively involved in the grain size but mainly determined by dislocation density and the distribution of second phase particles during FSW. Sub-grain boundaries between 2° and 5° are bound up with dislocation density.

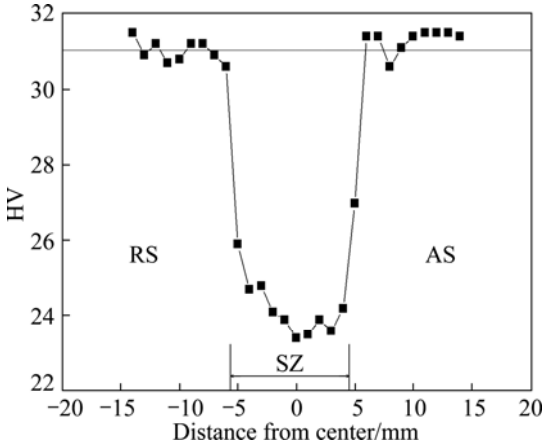

Fig. 6 Hardness profile in transversal section for different locations

Figures. 3(d)−(f) show that the contents of sub-grain boundaries between 2° and 5° in SZ are lower than those in BM. It is revealed that the dislocation density is greatly decreased after FSP, resulting in the reduction of hardness. From Figs. 3(b), (c), (g) and (h), no obvious difference of content of sub-grain boundaries between 2° and 5° is observed in TMAZ and HAZ compared to those in BM, and the hardness almost keeps the same as that in the BM. So the hardness curve of the transversal section shows a “U” shape. For aluminum alloys, the hardness curve shows a “W” shape [7−11], which has been explained to be that the hardness is mainly depended on the precipitate distribution. The dissolution of the precipitate during FSP results in the low hardness in the processed region, and the improved hardness in the SZ compared to those in the TMAZ and HAZ is attributed to the re-precipitation after FSP. This process leads to the “W” shape of the hardness curve. But for pure aluminum, there is almost no precipitation except the influence of the impurities. So the hardness is improved due to the fact that the re-precipitation does not exist in the SZ, generating the “U” shape of hardness curve.

The hardness curve is asymmetric and the lowest hardness is observed in the center of the SZ. In the SZ, the average hardness of the RS is slightly higher than that of the AS, which contributes to higher fraction of sub-grain boundaries of the RS than that of the AS. The softened region of RS is slightly wider than that of AS. This phenomenon is in accordance with the macroscopic structure of the transversal section where the slope of AS is larger than that of RS, as shown in Fig. 1. This is mainly affected by the tilted tool and different material flow between the two sides.

4 Conclusions

1) In the stir zone (SZ), fine equiaxed grains are obtained due to complete recrystallization. The thermo-mechanically affected zone (TMAZ) contains few equiaxed grains due to insufficient deformation strain. Heat-affected zone (HAZ) retains the same banded structure as the base material.

2) In the center of SZ, the dominant texture component is (111) parallel to about 70° from ND pointing toward the direction of the RD. The texture of this location rotates clockwise about 30° and anticlockwise about 60° around the ND resulting in the texture of the areas, which is 3 mm apart from it on the RS and AS, respectively. The texture component of the base material mainly consists of R, S and brass R textures. The same texture component as the base material is found in the TMAZ and HAZ, but it is a little weaker than in the base material.

3) The hardness curve shows a “U” shape due to a local material softening occurring in the SZ, because of the heat produced by the FSP.

References

[1] MISHRA R S, MA Z Y. Friction stir welding and processing [J]. Materials Science and Engineering R, 2005, 50(1): 1−78.

[2] BENAVIDES S, LI Y, MURR L E, BROWN D, MCCLURE J C. Low-temperature friction-stir welding of 2024 aluminum [J]. Scripta Materialia, 1999, 41(8): 809−815.

[3] MURR L E, LI Y, FLORES R D, TRILLO E A, MCCLURE J C. Intercalation vortices and related microstructural features in the friction-stir welding of dissimilar metals [J]. Material Research Innovations, 1998, 2(3): 150−163.

[4] FONDA R W, KNIPLING K E, BINGERT J F. Microstructural evolution ahead of the tool in aluminum friction stir welds [J]. Scripta Materialia, 2007, 58(5): 343−348.

[5] SATO Y S, KOKAWA H, IKEDA K, ENOMOTO M, JOGAN S, HASHIMOTO T. Microtexture in the friction-stir weld of an aluminum alloy [J]. Metallurgical and Materials Transactions A, 2001, 32(4): 941−947.

[6] SUHUDDIN U F H R, MIRONOV S, SATO Y S, KOKAWA H. Grain structure and texture evolution during friction stir welding of thin 6016 aluminum alloy sheets [J]. Materials Science and Engineering A, 2010, 527(7): 1962−1969.

[7] KANG J, LUAN G, FU R. Microstructures and mechanical properties of banded textures of friction stir welded 7075-T6 aluminum alloy [J]. Acta Metallurgica Sinica, 2011, 47(2): 224−230. (in Chinese)

[8] REDDY G M, MASTANAIAH P, PRASAD K S, MOHANDAS T. Microstructure and mechanical property correlations in AA6061 aluminum alloy friction stir welds [J]. Transactions of the Indian Institute of Metals, 2009, 62(1): 49−58.

[9] CHEN Y C, FENG J C, LIU H J. Precipitate evolution in friction stir welding of 2219-T6 aluminum alloys [J]. Materials Characterization, 2009, 60(6): 476−481.

[10] FONDA R W, BINGERT J F. Precipitation and grain refinement in a 2195 Al friction stir weld [J]. Metallurgical and Materials Transactions A, 2006, 37(12): 3593−3604.

[11] STARINK M J, DESCHAMPS A, WANG S C. The strength of friction stir welded and friction stir processed aluminum alloys [J]. Scripta Material, 2008, 58(5): 377−382.

[12] YADAV D, BAURI R. Effect of friction stir processing on microstructure and mechanical properties of aluminum [J]. Materials Science and Engineering A, 2012, 539: 85−92.

[13] SATO Y S, KOKAWA H, MASATOSHI E, JOGAN S. Microstructural evolution of 6063 aluminum during friction-stir welding [J]. Metallurgical and Materials Transactions A, 1999, 30(9): 2429−2437.

[14] AGARWAL S, BRIANT C L, HECTOR L G, CHEN Y L. Friction stir processed AA5182-O and AA6111-T4 aluminum alloys. Part 1: Electron backscattered diffraction analysis [J]. Journal of Materials Engineering and Performance, 2007, 16(4): 391−401.

[15] LI Y, MURR L E, MCCLURE J C. Flow visualization and residual microstructures associated with the friction-stir welding of 2024 aluminum to 6061 aluminum [J]. Materials Science and Engineering A, 1999, 271(1): 213−223.

[16] MA Z Y, MISHRA R S, MAHONEY. Superplastic deformation behavior of friction stir processed 7075Al alloy [J]. Acta Materialia, 2002, 50(17): 4419−4430.

[17] SU J Q, NELSON T W, STERLING C J. Microstructure evolution during FSW/FSP of high strength aluminum alloys [J]. Materials Science and Engineering A, 2005, 405(1): 277−286.

[18] BLUM W, ZHU Q, MERKEL R, MCQUEEN H J. Geometric dynamic recrystallization in hot torsion of Al−5Mg−0.6Mn (AA5083) [J]. Materials Science and Engineering A, 1996, 205(1): 23−30.

[19] FIELD D P, NELSON T C, HOVANSKI Y, JATA K V. Heterogeneity of crystallographic texture in friction stir welds of aluminum [J]. Metallurgical and Materials Transactions A, 2001, 32(11): 2869−2877.

[20] AHMED M M Z, WYNNE B P, RAINFORTH W M, THREADGILL P L. Through-thickness crystallographic texture of stationary shoulder friction stir welded aluminum [J]. Scripta Materialia, 2011, 64: 45−48.

[21] AHMED M M Z, WYNNE B P, RAINFORTH W M, THREADGILL P L. Quantifying crystallographic texture in the probe-dominated region of thick-section friction-stir-welded aluminum [J]. Scripta Materialia, 2008, 59: 507−510.

[22] SATO Y S, KURIHARA S, KOKAWA H. Systematic examination of precipitation phenomena associated with hardness and corrosion properties in friction stir welded aluminum alloy 2024 [J]. Welding in the World, 2011, 55(11−12): 39−47.

纯铝搅拌摩擦加工后微观组织及硬度的演化规律

甘文英，周 正，张 航，彭 涛

重庆大学 材料科学与工程学院，重庆 400044

摘 要：研究轧制态纯铝经搅拌摩擦加工后的微观组织、织构及硬度。采用 EBSD 技术表征横截面的微观组织及织构。结果表明：焊合区晶粒呈等轴的完全再结晶状。基材主要包含的织构组分有 R、S 及黄铜 R，同时含有少量的铜型织构。在焊合区中心，主要的织构组分是平行于 ND 指向 RD 70°方向的(111)，这一区域的织构绕着 ND 顺时针旋转 30°和逆时针旋转 60°分别得到回退侧和前进侧距离此区域 3 mm 的织构。

关键词：搅拌摩擦加工；纯铝；EBSD；织构

(Edited by Chao WANG)